Vertical Structure and Energetics of the Western Pacific Teleconnection Pattern

Sho Tanaka, Kazuaki Nishii*, and Hisashi Nakamura

Research Center for Advanced Science and Technology, the University of Tokyo, Tokyo, Japan

*Current affiliation: Graduate School of Bioresources, Mie University, Tsu, Japan.

Corresponding author: Kazuaki Nishii (nishii@bio.mie-u.ac.jp)

Department of Environmental Science and Technology, Graduate School of Bioresources, Mie University, 1577 Kurimamachiya-cho, Tsu, 514-8507, Japan

Submitted to Journal of Climate in August 2015.

Revised in November 2015, March 2016, and June 2016.

Abstract

The Western Pacific (WP) pattern, characterized by north-south dipolar anomalies in pressure over the Far East and western North Pacific, is known as one of the dominant teleconnection patterns in the wintertime Northern Hemisphere. Composite analysis reveals that monthly height anomalies exhibit baroclinic structure with their phase lines tilting southwestward with height in the lower troposphere. The anomalies can thus yield not only a poleward heat flux across the climatological thermal gradient across the strong Pacific jet but also a westward heat flux across the climatological thermal gradient between the North Pacific and the cooler Asian Continent. The resultant baroclinic conversion of available potential energy (APE) from the climatological-mean flow contributes most efficiently to the APE maintenance of the monthly WP pattern, acting against strong thermal damping effects by anomalous heat exchanges with the underlying ocean and anomalous precipitation in the subtropics and by the effect of anomalous eddy heat flux under modulated stormtrack activity. Kinetic energy (KE) of the pattern is maintained through barotropic feedback forcing associated with modulated activity of transient eddies and the conversion from the climatological-mean westerlies, both of which act against frictional damping. The net feedback forcing by transient eddies is therefore not particularly efficient. The present study suggests that the WP pattern has a characteristic of a dynamical mode that can maintain itself through efficient energy conversion from the climatological-mean fields even without external forcing, including remote influence from the Tropics.

1. Introduction

The Western Pacific (WP) pattern is a tropospheric teleconnection pattern characterized by a north-south dipole of geopotential height anomalies over the Far East and western North Pacific (Wallace and Gutzler 1981; hereafter WG81). The WP pattern is known as one of the teleconnection patterns that modulate the East Asian winter monsoon (Takaya and Nakamura 2005a, 2005b, 2013), but its influence is not limited to the winter monsoon. Pavan et al. (2000) and Rivière (2010) showed that frequency of blocking or Rossby wave breaking occurrence over the North Pacific increases in months when the positive phase of the WP pattern is observed. (Note that the positive phase of the WP pattern is defined when the northern height anomaly is positive in this study, following the definition of WG81.) In fact, Takaya and Nakamura (2005b) pointed out that the evolution of a strong positive event of the WP pattern can typically be viewed as a cyclonic breaking of the upper-tropospheric planetary-wave trough (cf. Rivière 2010).

Linkin and Nigam (2008) identified the WP pattern with the North Pacific Oscillation (Walker and Bliss 1931; Rogers 1981; hereafter NPO). Referring to the joint pattern as NPO/WP, they argued that its impact on surface air temperature variability over the North America is comparable to that of the Pacific North American pattern (WG81; hereafter PNA) and El Niño/Southern Oscillation (ENSO; Walker and Bliss 1931; Horel and Wallace 1981). They also argued that its influence on variability of the Arctic Sea ice is stronger than that of other teleconnection patterns (In section 2, we will briefly discuss the relationship between the WP pattern and NPO).

Linkages between the WP pattern and ENSO have been known since Horel and Wallace (1981). In fact, the linkage between the positive WP pattern and La Niña was confirmed by Koide and Kodera (1999) as the third mode of singular value decomposition (SVD) between the global mid-tropospheric geopotential height and sea-surface temperature (SST) anomalies in boreal winter. However, Kodera (1998) and Ose (2000) argued that the WP-ENSO linkage may also be affected by other processes, including variability in snow cover over Siberia and precipitation over the South China Sea. Influence of midlatitude SST variability on the WP pattern has also been discussed. Hirose et al. (2009) showed that increasing transport in autumn of the Tsushima warm current, which brings warm water from the Kuroshio into the Sea of Japan through the East China Sea, tends to be linked with the positive phase of the WP pattern in winter. By prescribing SST anomalies in the Sea of Japan as the boundary condition for a regional atmospheric model, Yamamoto and Hirose (2011) obtained an atmospheric response similar to the WP pattern.

Frankignoul et al. (2011) identified circulation anomalies like the WP pattern in association with the decadal SST variability in the Kuroshio-Oyashio Extension (KOE). The WP and PNA patterns alter the position of the surface Aleutian Low and change surface wind stress curl over the North Pacific, which forces westward-propagating oceanic baroclinic Rossby waves to displace the northern boundary of the North Pacific subtropical gyre and thereby alter SST in the KOE region (Ishii and Hanawa 2005; Sugimoto and Hanawa 2009). Furthermore, an atmospheric global circulation model (AGCM) experiment with SST anomalies over the midlatitude North Pacific can simulate tropospheric height anomalies like the WP pattern and a cooling in the polar stratosphere (Hurwitz et al. 2012). In fact, Orsolini et al. (2009) and Nishii et al. (2010) demonstrated that the positive WP pattern acts to lower the polar stratospheric temperature over the Arctic and thereby increase polar stratospheric clouds through suppression of upward planetary waves into the stratosphere.

Some previous studies attempted to interpret the dynamics of the WP pattern from a viewpoint of an internal dynamical mode of the midlatitude atmosphere that can be excited even without external forcing like ENSO. Nakamura et al. (1987) argued that kinetic energy (KE) conversion from the climatological-mean flow to the WP pattern might be less efficient than that to the PNA pattern, in recognition of the fact that the PNA pattern is located in the exit of the Pacific jet but the WP pattern is not. Rather, the WP pattern is close to the core of the Pacific stormtrack and thus may be effective in modulating transient eddy activity (Nakamura et al. 1987). In fact, Lau (1988) and Lau and Nath (1991) concluded that barotropic feedback forcing from synoptic-scale transient eddies can be efficient for the maintenance of the WP pattern. Consistently, Li and Wettstein (2012) argued that the Pacific jet variability associated with the WP pattern shows eddy-driven signature, in contrast to the jet variability associated with the PNA pattern that shows more thermally-driven signature.

Most of the previous studies on low-frequency atmospheric variability, including the WP and PNA teleconnection patterns, have focused on barotropic processes. This may be because circulation anomalies associated with low-frequency variability appear to be equivalent barotropic, especially over the oceans (e.g., Blackmon et al. 1979; Hsu and Wallace 1985). Black and Dole (1993) and Black (1997) pointed out, however, that height anomalies in association with the PNA pattern exhibit a westward phase tilt with height and thus baroclinic processes may contribute to the development of the PNA pattern. Linkin and Nigam (2008) also found height anomalies associated with the WP pattern to be in baroclinic structure with a westward phase tilt with height. In summer, the Pacific-Japan (PJ) pattern, a teleconnection pattern characterized by meridionally aligned height anomalies over the Far East and western North Pacific (Nitta 1987), exhibits baroclinic structure with a northwestward phase tilt with height (Kosaka and Nakamura 2006, 2010). The PJ pattern thus accompanies northward and eastward heat fluxes, acting to relax thermal contrasts between the warmer Asian continent associated with the summer monsoon and the climatologically cooler Siberia and North Pacific to the north and east, respectively. These down-gradient heat fluxes act to reinforce the PJ pattern through conversion of available potential energy (APE) from the climatological-mean flow. The baroclinic structure of the PJ pattern in summer motivates us to investigate the vertical structure and energetics of the wintertime WP pattern. As the zonal thermal contrast is reversed from summer to winter, height anomalies associated with the WP pattern may exhibit a southward phase tilt with height to yield a westward heat flux, in contrast to the PJ pattern. We will show that is indeed the case for the WP pattern through composite analysis for its high-amplitude monthly events based on reanalysis data. We will also show that the WP pattern can thus maintain itself mainly through APE conversion against dissipation processes.

2. Data and analysis procedure

In the present study, monthly-mean data and 6-hourly data based on the European Centre for Medium-Range Weather Forecasts (ECMWF) Reanalysis Interim (ERA-Interim; Dee et al. 2011) are used. The horizontal resolution of the data is 0.75° x 0.75° in longitude and latitude. We analyzed 32 winters (DJF) from 1979/80 through 2010/11. Diabatic heating was estimated locally as the residual of the thermodynamic equation based on 6-hourly data. For the analysis of the earlier period 1948/49-1978/79, we use another reanalysis dataset provided by the National Centers for Environmental Prediction (NCEP) and the National Center for Atmospheric Research (NCAR) (NCEP–R1; Kalnay et al. 1996). All the results shown in this paper are based on the ERA-Interim unless otherwise stated.

Sub-weekly fluctuations associated with synoptic-scale transient eddies have been extracted through digital high-pass filtering with a half-power cutoff period of 8 days, following Kushnir and Wallace (1989) and Nakamura et al. (2002). In the following, the fluctuations thus obtained are denoted by double primes. Momentum and heat fluxes associated with the transient eddies (e.g., zonal momentum flux ($u''v''$) and meridional heat flux ($v''T''$)) have been 8-day low-pass filtered and then averaged monthly at each grid point before being used in the following composite analysis. (The 8-day low-pass filtering prior to taking monthly averaging does not affect our results. The filtered data was prepared for the sake of other studies.) We also used precipitation data provided by Global Precipitation Climatology Project (GPCP; Adler et al. 2003), whose resolution is 2.5° x 2.5°. HadISST (Rayner et al. 2003) is used for SST and its resolution is 2.5°x2.5°.

The following WP pattern index (hereafter WP index) defined by WG81 is used in this study:

$$WP\ index = \frac{1}{2}\{Z_{500}(60N, 155.25E) - Z_{500}(30N, 155.25E)\} \qquad (1)$$

In (1), Z_{500} represents a monthly-mean anomaly of 500-hPa geopotential height normalized by its standard deviation at a given location for each calendar month. Note that the grid points used in (1) are to the east of their counterpart in WG81 by 0.25°. The anomaly of a given variable for a given month is defined as a local deviation from its 32-year climatological mean for the particular calendar month. The index is suitable for extracting a signature of dipolar height anomalies over the western North Pacific. In our definition, the positive phase of the WP pattern corresponds to cyclonic and anticyclonic anomalies at the southern and northern centers of action, respectively, and vice versa for the negative phase, as in the definition by WG81. Composite maps of various anomalous fields are constructed separately for the positive and negative phases of the WP pattern. For our composites of strong positive WP events, 18 months are selected for which the WP index is positive and exceeds a unit standard deviation in strength (Table 1). Likewise, 14 months are selected for strong negative WP events. In the following, we use the term "event" to denote a selected month. Refer to section 5 for the discussion on the usage of monthly data for the analysis of the WP pattern instead of daily data.

Linkin and Nigam (2008) argued that the WP pattern is identical to the NPO, posing a question on the appropriateness of the usage of the particular WP index in our analysis. For verification, we construct “teleconnectivity maps” for monthly anomalies of 500-hPa height for boreal winter (DJF), following WG81 but separately for the periods 1962/63–1976/77 (Fig. 1a) and 1948/49–2010/11 (Fig. 1b) based on the NCEP-R1 data. In each of the maps, what is plotted at a given location is “teleconnectivity”, defined as the absolute value of the strongest negative correlation obtained in height anomalies between the particular location and any of the other locations for the 45 months during a given 15-year period. Locations of strong teleconnectivity are thus likely to correspond to centers of action of pressure seesaws. Constructed for the same period as in WG81, the teleconnectivity map shown in Fig. 1a is very similar to their Fig. 7b, in which the two centers of action of the WP pattern are unambiguously depicted as local maxima of teleconnectivity (as indicated in Fig. 1a with red crosses). Two other local maxima in Fig. 1a correspond to centers of action of the PNA pattern, one over the central North Pacific and the other over western North America. Figure 1a suggests that in the particular period height variability associated with the WP pattern was as prominent as that with the PNA pattern.

In the corresponding map for 1948/49–2010/11 winters (Fig. 1b), by contrast, the teleconnectivity maxima that correspond to the WP pattern cannot be identified. We speculate that the missing teleconnectivity maxima associated with the WP pattern in Fig. 1b may be due to the dominant variability associated with the PNA pattern over that with the WP pattern in the statistics for the 62-year period. Then, the centers of action of the WP pattern would possibly emerge in the teleconnectivity map if the variability associated with the PNA pattern were statistically removed in the calculation of the teleconnectivity. To verify this possibility, we first define the following PNA index:

$$PNA\ index = \frac{1}{2}\{Z_{500}(20N, 180E) - Z_{500}(50N, 190E)\} \quad . \quad (2)$$

Note that the two reference grid points in (2) are shifted slightly from their counterpart in WG81, so as to correspond to the centers of action of the PNA pattern in the period 1948/49–2010/11 recognized as the teleconnectivity maxima in Fig. 1b.

To remove the dominant signal of the PNA pattern, we used partial correlation where variability correlated with the PNA index has been removed before evaluating teleconnectivity. See Appendix A for more detail. As shown in Fig. 1c, the signature of the PNA pattern over the North Pacific is therefore no longer recognized. Instead, four teleconnectivity maxima are identified within the North Pacific, and two of them are located in the immediate vicinities of the centers of action of the WP pattern (red crosses). We have confirmed that strong negative correlation is indeed observed between height anomalies at these two locations. The two other teleconnectivity maxima around 160°W (blue crosses in Fig. 1c) may correspond to centers of action of another teleconnection pattern. This pattern, if it actually exists, is located so close to the WP pattern that the two patterns cannot be spatially orthogonal. It is therefore unlikely that they are extracted in separate modes of variability through an empirical orthogonal function (EOF) analysis, as used by Linkin and Nigam (2008) for identifying the NPO/WP pattern. Recognizing the clear signature of the WP pattern in Fig. 1c, we use the WP index based on its definition as in (1) throughout this study. In doing so, we expect the obtained variability to be more geographically fixed than that obtained through EOF analysis.

The other teleconnection pattern suggested in Fig. 1c may be similar to the NPO, although a detailed comparison between the NPO and WP pattern is beyond the scope of this study. The comparable dominance of the WP pattern to the PNA pattern for the period of 1962/63–1976/77 (Fig. 1a) may suggest possible long-term modulations of the WP pattern, which is also beyond the scope of this study.

3. Three-dimensional structure of the WP pattern

As shown in Fig. 2a, 500-hPa height anomalies composited for the 18 strongest monthly events of the positive WP pattern are characterized by a north-south dipole, in good agreement with WG81. The northern anticyclonic anomaly is over eastern Siberia, the Kamchatka Peninsula and Sea of Okhotsk, while the southern cyclonic anomaly is elongated zonally from the Far East to as far as the Hawaiian Islands. The center of the latter anomaly does not coincide with the southern reference grid point for the WP index (southern green point in Fig. 2a), but it shifts slightly northeastward. This may be because the intraseasonal and interannual variance of 500-hPa height in winter is larger over the eastern North Pacific than over the central and western North Pacific (Blackmon et al. 1984).

A zonal-height section for 30˚N (Fig. 2c), the latitude very close to that of the center of the southern anomaly of the WP pattern, shows that the phase of the composited height anomaly tilts westward with height in the lower and mid-troposphere.

Furthermore, a meridional cross-section for 155˚E (Fig. 2e), the longitude of the two reference grid points for the WP index, shows a southward tilt of the height anomalies with height in the lower and mid-troposphere. The southward tilt in the mid-troposphere may not necessarily be unambiguous, but it is consistent with westward heat flux, as shown in Fig. 6c. This baroclinic structure of the WP pattern differs from the findings by the previous studies that show equivalent barotropic structure of low-frequency variability over the oceans (e.g., Blackmon et al. 1979; Hsu and Wallace 1985). The apparent barotropic structure of low-frequency anomalies may be due to coarse horizontal and vertical resolutions of observational data at that time. In fact, some previous studies pointed out that baroclinic structure of the WP and PNA patterns is manifested as a westward phase tilt with height (e.g., Black and Dole 1993; Black 1997; Linkin and Nigam 2008). However, the southward phase tilt has never been pointed out. This baroclinic structure implies baroclinic energy conversion from the climatological-mean flow into the WP pattern, which will be quantified in section 4.

As the composite anomalies of the negative WP pattern (Figs. 2b, d, f) look almost like a mirror image of their positive counterpart (Figs. 2a, c, e), we focus only on its positive phase in the following. In the positive WP pattern, a cold anomaly with the enhanced northwesterlies is observed near the surface over the East China Sea and south of Japan (Fig. 3a). This is consistent with Takaya and Nakamura (2005a, b), who pointed out that a blocking high whose height anomaly has a strong projection onto the WP pattern tends to amplify the surface Siberian High and thereby give rise to a cold surge over East Asia. Cold anomalies with the anomalous westerlies are also observed in the lower and mid-troposphere over the East China Sea and south of Japan (Figs. 3b-c). Around the Sea of Okhotsk, by contrast, a warm anomaly is observed with anomalous easterlies in the lower and mid-troposphere (Figs. 3b-c). These wind and temperature anomalies are consistent with the baroclinic structure of the WP pattern with a southward phase tilt (Fig. 2e) and equivalent to a westward heat flux (Fig. 3c). Acting on the zonal gradient in climatological temperature between the warmer Pacific and cooler Asian Continent, this westward heat flux is down-gradient and thus implies baroclinic energy conversion from the climatological-mean flow to the WP pattern.

In the upper troposphere (Fig. 3d), the positive WP pattern accompanies anomalous easterlies and westerlies to the north and south, respectively, which suggests southward shift of the jetstream over the western North Pacific. The midlatitude anomalous easterlies are consistent with the suppression of stormtrack activity, as indicated by anomalous lower-tropospheric poleward heat flux associated with sub-weekly disturbances (Fig. 3e) and by upper-tropospheric variance of sub-weekly fluctuations in the meridional wind velocity (Fig. 3f). The weakening of the stormtrack activity is consistent with the relaxed tropospheric meridional temperature gradient in association with the positive WP pattern (not shown).

Diabatic heating anomalies associated with the WP pattern are observed mainly in the lower and mid-troposphere. In the lower troposphere, a positive anomaly of diabatic heating is observed over the midlatitude/subtropical North Pacific, while a negative anomaly is over the Sea of Okhotsk and Bering Sea (Fig. 4a). The former and latter anomalies seem consistent with the local enhancement and reduction, respectively, of sensible heat flux (SHF) from the ocean to the atmosphere (Fig. 4c). As diabatic heating of the ERA-Interim reanalysis dataset is not available, we analyzed two other reanalysis datasets of NCEP-R1 and JRA-25 (Onogi et al. 2007) that provide diabatic heating data. We have confirmed that those diabatic heating anomalies are mainly due to anomalous vertical diffusion (not shown), which is consistent with our speculation. Induced by strengthening and weakening of cold air outflow from the continent (Figs. 3a-b), the enhancement and reduction of upward SHF, respectively, associated with the WP pattern act to cool and warm the ocean surface over the respective domains and thereby force the SST anomalies as observed (Fig. 4b). In fact, those SST anomalies are hardly observed in the preceding months of the positive WP events selected for the compositing (not shown). A recent numerical study has suggested that SST anomalies similar to Fig. 4b can generate anomalous atmospheric circulation like the positive WP pattern (Hurwitz et al. 2012). Thus, there may be positive feedback between the WP pattern and associated SST anomalies. In the mid-troposphere, a positive diabatic heating anomaly observed over the eastern North Pacific (Fig. 4d) corresponds to enhanced precipitation (Fig. 4e), which is mainly due to enhanced convective heating, as represented in the NCEP-R1 and JRA-25 data. The enhanced convective precipitation around 30°N is consistent with reduced static stability associated with the cyclonic anomaly (Figs. 3b-c).

4. Energetics of the WP pattern

To examine mechanisms for the maintenance of the monthly anomalies associated with the WP pattern, we quantify each of the energy conversion/generation terms relevant to the WP pattern based on its composited anomalies. Making composite maps based on all the selected WP pattern events should suppress circulation anomalies that were unrelated to the WP pattern in the individual months, often observed far from the North Pacific. This procedure is necessary for our assessment of the energetics of the WP pattern. If energetics were evaluated for the individual events before making composite, those circulation anomalies unrelated to the WP pattern could contribute to the energy conversion/generation terms that are essentially quadratic with respect to local anomalies and the energetics evaluated could therefore be substantially contaminated.

Barotropic energy conversion (or KE conversion; *CK*) from the climatological-mean flow into the anomalies associated with the WP pattern has been estimated, as in Hoskins et al. (1983), Simmons et al. (1983), and Kosaka and Nakamura (2006, 2010):

$$CK = \frac{v'^2 - u'^2}{2}\left(\frac{\partial \bar{u}}{\partial x} - \frac{\partial \bar{v}}{\partial y}\right) - u'v'\left(\frac{\partial \bar{u}}{\partial y} + \frac{\partial \bar{v}}{\partial x}\right). \quad (3)$$

Here, the overbars and primes denote climatological-mean quantities and monthly-mean anomalies, respectively, and positive *CK* means that KE, defined as $(u'^2 + v'^2)/2$ for the anomalies, is converted from the climatological-mean flow into the anomalies. Refer to Appendix B for the derivation of (3). Figure 5 shows a map of *CK* evaluated at the 250-hPa level, where horizontal wind shear is particularly strong climatologically along the Pacific jet. As shown in Fig. 5a, positive *CK* maxima are observed to the northern and southern flanks of the Pacific jet downstream of its core region. The first term of

CK in (3), hereafter referred to as *CKx*, contributes positively to *CK* on the northern and southern portions of the jet exit region (Fig. 5b), where anomalous easterlies and westerlies, respectively, induce anomalous advection of the climatological westerly momentum ($-u'\,\partial\bar{u}/\partial x$) that acts to reinforce themselves. The second term of *CK* in (3), hereafter referred to as *CKy*, also contributes positively in the southern portion of the jet exit (Fig. 5c), where the anomalous winds have a slight northerly component and thus yield anomalous advection of climatological westerly momentum across the meridional shear of the climatological jet ($-v'\,\partial\bar{u}/\partial y$) that acts to reinforce the anomalous winds. Positive *CKy* is also observed on the northern flank of the jet core, across which the anomalous northeasterlies yield anomalous easterly advection to reinforce themselves.

Baroclinic energy conversion (*CP*) through which APE, defined for the anomalies as $(R/pS_p)(T'^2/2)$, is converted from the climatological-mean state to the monthly anomalies is estimated, as in Kosaka and Nakamura (2006, 2010):

$$CP = -\frac{R}{pS_p}\left(u'T'\frac{\partial\bar{T}}{\partial x} + v'T'\frac{\partial\bar{T}}{\partial y}\right). \qquad (4)$$

Here, $S_p = (R/p)\,[(RT/pC_p) - dT/dp]$ evaluated for the climatological-mean state, where R and C_p denote the gas constant and the specific heat at constant pressure (p), respectively. Figures 6a and 6b show maps of *CP* evaluated at the 500 and 850-hPa levels, respectively, for the positive WP pattern, Positive *CP* maxima are evident to the south of the northern reference point and to the west of the southern reference point of the WP pattern. The northern and southern *CP* maxima are mainly contributed to by the first (*CPx*) and second *(CPy)* terms, respectively, of (4). Around the northern *CP* maximum around the Sea of Okhotsk and western Bering Sea, background zonal temperature gradient is strong associated with the climatological-mean planetary waves (Fig. 6c) and thermal contrasts between the warmer Pacific Ocean and colder Eurasian continent (Fig. 6d). Acting on this temperature gradient, the westward heat flux, which reflects the southward-tilting height anomalies as discussed before (Figs. 2e and 3c), yields large positive *CP*. Contrastingly around the southern *CP* maximum over the midlatitude/subtropical western Pacific, APE is converted mainly through poleward heat flux acting on the climatologically strong temperature gradient (Fig. 6c) accompanied by the Pacific jet (Fig. 3c). The poleward heat flux is consistent with baroclinic structure of the WP pattern with the westward-tilting height anomalies (Fig. 2e). In the lower troposphere (Fig. 6b), those positive *CP* maxima are contributed to also by relatively low static stability (i.e., small S_p), which arises climatologically from the monsoonal outflow of cold continental air onto the warmer ocean. It should be noted that negative *CP* values, which are particularly noticeable in Fig. 6a, are quite small and therefore make no significant contributions to the hemispherically integrated *CP*.

Anomalous APE generation by anomalous diabatic heating (*CQ*) is defined as,

$$CQ = \frac{R}{pC_pS_p}T'Q', \qquad (5)$$

where Q on the RHS denotes diabatic heating. In the mid-troposphere (Fig. 7a), negative *CQ* over the central/eastern North Pacific south of 40°N results from anomalous diabatic warming due to increased precipitation (Figs. 4d-e) over the cold cyclonic anomaly of the WP pattern (Fig. 3c). In the lower troposphere (Fig. 7b), warm and cold anomalies tend to be damped by heat exchanges with the underlying ocean in the form of negative and positive SHF anomalies, respectively (Figs. 3b and 4c), yielding negative *CQ* (Fig. 7b). Those anomalies in air temperature and SHF arise from modulated cold surges in association with the positive WP pattern, as mentioned in the preceding section.

Previous studies pointed out the importance of feedback forcing from transient eddies in the maintenance of the WP pattern (Nakamura et al. 1987; Lau 1988). The KE and APE gains for the monthly WP pattern due to modulated activity of high-frequency transient eddies can be evaluated as follows;

$$CK_{HF} = -u'\left(\frac{\partial(u''u'')'}{\partial x} + \frac{\partial(u''v'')'}{\partial y}\right) - v'\left(\frac{\partial(u''v'')'}{\partial x} + \frac{\partial(v''v'')'}{\partial y}\right), \qquad (6)$$

$$CP_{HF} = -\frac{RT'}{pS_p}\left(\frac{\partial(u''T'')'}{\partial x} + \frac{\partial(v''T'')'}{\partial y}\right). \qquad (7)$$

In (6) and (7), the double primes denote 8-day high-pass-filtered, sub-weekly fluctuations associated with transient eddies, and their products implicitly denote monthly statistics. Refer to Appendix A for the derivation of (6), and (7) can be derived in a similar manner. Hereafter, the KE and APE gains defined as (6) and (7) are referred to as barotropic feedback (CK_{HF}) and baroclinic feedback (CP_{HF}), respectively.

Figure 8a shows CK_{HF} at the tropopause level, where not only the monthly wind anomalies but also sub-weekly wind fluctuations tend to be larger than at any other levels. In agreement with previous studies (Lau 1988; Lau and Nath 1991), upper-tropospheric CK_{HF} contributes overall positively to the maintenance of the monthly WP pattern by acting to increase KE over the central and eastern North Pacific (Fig. 8a), most prominently in the downstream portion of the stormtrack core. Since synoptic-scale eddies migrating along the stormtrack act to accelerate the westerlies through converging eddy momentum fluxes, the weakening of the stormtrack activity associated with the positive WP pattern induces anomalous easterly acceleration with anomalous divergence of eddy momentum flux where the monthly anomalies are easterly (Fig. 8c). Likewise, anomalous convergence of a southerly momentum flux associated with transient eddies that acts to reinforce the anomalous southerlies over the eastern North Pacific contributes positively to CK_{HF} (Fig. 8e).

In contrast to CK_{HF}, CP_{HF} overall contributes negatively to the maintenance of the monthly WP pattern (Fig. 8b), as anomalous heat flux associated with transient eddies is generally down-gradient and thus acting to relax anomalous temperature gradient associated with the monthly WP pattern, as shown in the previous studies (e.g., Lau and Nath 1991). The weakening of the stormtrack activity associated with the positive WP pattern accompanies reduced poleward eddy heat flux associated with transient eddies (Fig. 3c), thereby yielding anomalous convergence and divergence of the flux where cold and warm anomalies are located to the south and north of the stormtrack axis, respectively (Fig. 8d). In this manner, transient eddies act to damp the monthly-mean thermal anomalies and thereby reduce APE associated with the WP pattern, in acting to render the monthly anomalies less baroclinic.

For a more quantitative assessment of the energetics for the monthly WP pattern, we integrated each of the energy conversion/generation terms horizontally over the entire extratropical Northern Hemisphere (20˚~90˚N, 0˚~360˚E) and vertically from the surface to the 100-hPa level. Dividing this value by the sum of KE and APE (i.e., the total energy) of the monthly WP pattern that has been integrated over the same three-dimensional domain yields the efficiency of each of those terms, which is shown in Table 2. In this table, a negative value signifies that the particular term contributes negatively to the maintenance of the WP pattern. It should be noted that energy flux terms on the RHS of (B9) in Appendix B, which represent energy redistribution by wavy anomalies and climatological-mean flow, should be negligible after integrated over the entire extratropical Northern Hemisphere. The third term on the RHS of (B9) represents energy conversion from APE to KE and therefore need not be discussed as long as the total energy is considered.

Among the several conversion/generation terms listed in Table 2, the process that can contribute to the maintenance of the total energy of the monthly WP pattern with the highest efficiency is baroclinic energy conversion (*CP*), through which the total energy of the WP pattern could be replenished within five days. Barotropic energy conversion (*CK*) can also contribute positively to the maintenance of the WP pattern, but its efficiency is less than one third of that of *CP*. Through their evaluation of *CK* and *KE* only at the 500-hPa level, Nakamura et al. (1987) argued that barotropic energy conversion may be important for the maintenance of the WP pattern, but the present study reveals the greater importance of baroclinic processes. In agreement with Lau (1988), barotropic feedback from transient eddies (CK_{HF}) is also important for the maintenance of the WP pattern, but its efficiency is only 40% of that of *CP*.

Furthermore, the net contribution from transient eddies is even less important; its efficiency is only 10% of that of *CP*, because of the large offset by the negative contribution through CP_{HF} (Lau and Nath 1991). When combined, all the energy conversion terms with the climatological-mean flow and transient eddies are highly efficient in the maintenance of the monthly anomalies of the WP pattern, as their total energy could be replenished within only three or four days. This efficiency appears to be sufficient for maintaining the WP pattern against thermal and frictional damping. As indicated in Table 2, anomalous diabatic heating as a net acts as thermal damping, through which the total energy can be consumed within 10 days. The efficiency of the frictional damping cannot be evaluated from the dataset. The same evaluation of the energetics has been repeated for the composited anomalies for the negative phase of the WP pattern, and qualitatively the same result is obtained as shown in Table 2.

Table 2 shows that the conversion from APE to KE (hereafter *CPK*), if integrated over the extratropical Northern Hemisphere within the full depth of the troposphere, is virtually zero for the positive phase of the monthly WP pattern and negligible for its negative phase. In agreement with previous studies, KE is maintained for the WP pattern primarily through barotropic feedback forcing from synoptic-scale transient eddies and also through KE conversion from the climatological westerlies. Reflecting the baroclinic nature of the WP pattern, associated APE is nevertheless comparable to KE (with only 10~20% difference), and APE is maintained solely by *CP* under the destructive contributions from transient eddies and diabatic processes.

In the present study, we use 8-day high-pass filtering to extract sub-weekly fluctuations associated with high-frequency transient eddies. We repeated the above evaluation based on (6) and (7), by using sub-monthly fluctuations defined locally as daily deviations from the monthly averages in place of sub-weekly fluctuations. The evaluation indicates that CK_{HF} thus evaluated contributes positively with efficiency of 0.09 and 0.05 (i.e., replenishing time scales of 11 and 20 days, respectively) for the positive and negative phases of the WP pattern, respectively. The efficiency is more or less comparable to its counterpart based on sub-weekly fluctuations (Table 2). The CP_{HF} based on sub-monthly fluctuations contributes negatively (-0.21 and -0.20 for the positive and negative phases, respectively) with efficiency that is about three times higher than that based on sub-weekly fluctuations. Thus the net contribution from sub-monthly fluctuations to the maintenance of the WP pattern is negative, which is in sharp contrast to that from sub-weekly fluctuations. Our evaluations therefore suggest that the counteracting effect of quasi-stationary sub-monthly fluctuations on the monthly WP pattern.

5. Summary and discussion

Through composite analysis, we have investigated three-dimensional structure of the WP pattern and evaluated the energetics of the composited monthly anomalies associated with the WP pattern to clarify the mechanisms of its maintenance. For the compositing, we selected high-amplitude monthly events of the WP pattern based on the index defined by WG81. At first glance, the anomalies appear to be in equivalent barotropic structure, but a close inspection reveals that it is in baroclinic structure with a southwestward phase tilt with height from the surface to the mid-troposphere. Although previous studies have suggested the baroclinic nature of the PNA and WP patterns with a westward phase tilt with height (Black and Dole 1993; Black 1997; Linkin and Nigam, 2008), the southward-tilting height anomalies of the WP pattern have not been pointed out.

Energetics of the WP pattern revealed in the present study indicates that baroclinic APE conversion from the climatological-mean flow to monthly-mean anomalies through a horizontal heat flux contributes most efficiently to the maintenance of the WP pattern owing to its baroclinic structure. Of particular importance is the westward component of the heat flux associated with the southwestward-tilting height anomalies of the WP pattern. The particular flux component, especially around the northern center of action, yields efficient APE conversion in acting on the eastward gradient of climatological-mean tropospheric temperature over the Far East. The eastward temperature gradient reflects thermal contrasts between the warmer Pacific Ocean and the colder Eurasian continent and the climatological-mean planetary waves. The southwestward-tilting height anomalies of the WP pattern also yield a poleward heat flux, which also contributes to the APE conversion, especially around the southern center of action, in crossing the strong southward temperature gradient associated with the Pacific jet. As its southern center of action is close to the jet core region, the WP pattern can induce barotropic KE conversion from the climatological Pacific jet as a positive contribution to the maintenance. Its efficiency is, however, found lower than that of the baroclinic conversion. More importantly, barotropic feedback forcing due to modulated activity of the Pacific stormtrack also contributes positively to the KE maintenance of the WP pattern. The net feedback forcing by transient eddies is, however, of secondary importance because of a large offset between the barotropic feedback through eddy momentum fluxes that acts to increase KE and the baroclinic feedback through eddy heat fluxes that acts to reduce APE. These processes, most importantly the baroclinic APE conversion from the climatological-mean flow, are so efficient for the maintenance of the monthly anomalies of the WP pattern against frictional and thermal damping that the total energy of the pattern could be replenished within four days. In fact, anomalous diabatic heating acts as an efficient damping process for the WP pattern, through enhanced precipitation within the cold cyclonic anomaly in the subtropical Pacific and through anomalous SHF from the ocean due to modulated monsoonal outflow from the Eurasian continent.

Our finding of efficient APE conversion from the wintertime climatological-mean flow suggests that the WP pattern has a characteristic of a dynamical mode that can maintain itself even without external forcing. The pattern thus owes its existence to the particular wintertime climatological-mean conditions over the Far East and the western North Pacific, as characterized by the strong Pacific jet and zonal thermal contrasts between the warmer Pacific and the cooler Asian continent. Recently, Kosaka and Nakamura (2006, 2010) have found that the summertime PJ pattern also has a characteristic of a dynamical mode. Both the WP and PJ patterns are characterized by meridional dipoles of zonally elongated height anomalies over the western North Pacific, and these anomalies are tilting westward with height to allow efficient APE conversion from the westerly Pacific jet. Interestingly, the height anomalies associated with the PJ pattern are also tilting northward with height, which yields eastward heat flux from the warmer Asian Continent into the cooler North Pacific in summer. The opposing meridional tilting of height anomalies between the WP and PJ patterns is consistent with the seasonal reversal of the thermal gradient between the Asian Continent and North Pacific, so as to yield down-gradient heat fluxes for the APE conversion for the maintenance of those patterns. Another distinction between the two teleconnection patterns can be found in the role of anomalous diabatic heating due to anomalous precipitation, which acts as thermal damping for the WP pattern but not for the PJ pattern. Rather, anomalous convective heating acts to generate APE for the PJ pattern, and anomalous surface winds act to enhance anomalous evaporation and anomalous moisture transport for sustaining anomalous convection (Kosaka and Nakamura 2006, 2010). We therefore argue that the wintertime WP pattern is a dry dynamical mode whereas the summertime PJ pattern is a moist dynamical mode.

The large contribution of the APE conversion shown in this study is apparently inconsistent with previous works that emphasize the role of barotropic dynamics in low-frequency variability (e.g., Robinson 1991; Feldstein 2003). Sheng and Dereme (1991), however, have estimated energy conversion in the whole troposphere over the entire Northern Hemisphere to show that APE conversion from the climatological-mean state to low-frequency variability (with periods longer than 10 days) is larger than the KE conversion from high-frequency eddies (with periods shorter than 10 days) to low-frequency variability. The findings in this study are consistent with their study, urging us to re-evaluate the role of APE conversion in other teleconnection patterns based on state-of-the-art atmospheric reanalysis data. Nevertheless, many of the previous works emphasized equivalent-barotropic structure of low-frequency variability and focus only on upper-tropospheric processes. Lau and Nath (1991) pointed out that a momentum-flux contribution by high-frequency transient eddies is larger in the upper troposphere than in the lower troposphere, while a heat-flux contribution by high-frequency transient eddies that is stronger in the lower troposphere tends to offset the momentum-flux contribution in the upper troposphere. This suggests that focusing only on an upper-tropospheric level is likely to overemphasize the role of high-frequency transient eddies in the maintenance of low-frequency variability.

While the climatological-mean jet over the North Pacific is considered as a merger between the subtropical and eddy-driven jets (Mohri 1953; Nakamura and Sampe 2002; Lee and Kim 2003; Nakamura et al. 2010), Li and Wettstein (2012) argued that the jet variability associated with the WP pattern shows eddy-driven characteristics. This may imply an important contribution from transient eddy activity to the maintenance of the WP pattern, which is consistent with positive CK_{HF} in our evaluation. The contribution is, however, not particularly large, presumably because the positive CK_{HF} is limited to the central and eastern portions of the midlatitude North Pacific (Fig. 8a). For further investigation, we plotted latitudinal profiles of the westerlies and the convergence of westerly momentum flux by high-frequency transient eddies for the western (155˚E) and central (190˚E) portions of the North Pacific (Fig. 9). Climatologically (Figs. 9a and 9d), the westerly momentum flux by transient eddies is convergent and divergent on the poleward and equatorward sides, respectively, of the climatological-mean westerly jet axis. This suggests the hybrid nature of the Pacific jet as a mixture of subtropical and eddy-driven jets at each of the two longitudes. In the central North Pacific, anomalies in the westerlies and eddy westerly acceleration overall show mutually coherent profiles for both the positive and negative phases of the WP pattern (Figs. 9e-f), which confirms the eddy-driven nature of the jet as was suggested by Li and Wettstein (2012). In contrast, the corresponding coherence is not evident in the western North Pacific (Figs. 9b-c), which indicates a weaker signature of an eddy-driven jet in agreement with smaller CK_{HF} over the western North Pacific (Fig. 8a). Nevertheless, along each of the meridians, the jet width is greater for the positive phase than for negative phase of the WP pattern, under the stronger stormtrack activity in the positive phase. The full widths at the half maximum of the westerly profiles at 155˚E are 18.0˚ and 15.75˚ in latitude for the positive and negative phases, respectively, of the WP pattern (Fig. 9a), while the corresponding values at 190˚E are 28.5˚ and 24.0˚ (Fig. 9d). The jet width fluctuations associated with the WP pattern are thus greater over the central Pacific than over the western Pacific. Nevertheless, the overall tendency for the Pacific jet to be wider with its stronger intensity is consistent with Nakamura and Sampe (2002). Likewise, the displacement of the jet axis between the positive and negative phases of the WP pattern is greater at 190˚E (5.25˚) than at 155˚E (3.00˚).

As shown in previous studies (Takaya and Nakamura 2005b; Rivière 2010), a typical time scale of individual events of the WP pattern is shorter than a month. The months selected for compositing in the present study may include multiple events of the

WP pattern with a particular sign. This study nevertheless focuses on the processes for the maintenance of the WP pattern through composite analysis of monthly anomalies, in order to compare our results with many previous works on teleconnection patterns based on monthly anomalies (e.g., WG81; Linkin and Nigam 2008; Kosaka and Nakmaura 2006, 2010). Furthermore, if daily data is used for compositing, one may argue that the baroclinic structure and associated APE conversion can arise from contamination of transient baroclinic eddies, even if we use low-pass filtering to suppress their signature.

For further deepening our understanding of the formation and decaying mechanisms of the WP pattern, we need to examine detailed time evolution of the WP pattern based on daily data, unlike the present analysis where monthly-mean data is used. This is because the formation and decaying mechanisms may be different from the maintenance mechanisms. Feldstein (2003) and Michel and Rivière (2011) studied time evolution of low-frequency anomalies over the North Atlantic. Their results suggest that low-frequency eddy vorticity flux associated with decaying anomalies tend to contribute negatively to the KE conversion, which appears to be inconsistent with our findings of the monthly WP anomalies. Their results imply that, as they decay, low-frequency anomalies may change their horizontal structure and/or their positions relative to the climatological-mean westerly jet streams. In the present study, we focus on persistent circulation anomalies of the WP pattern extracted in monthly-mean fields whose horizontal structure is assumed to be unchanged. Obviously, this assumption is not valid for sub-monthly events of the positive WP pattern, which can be viewed as cyclonic breaking of the planetary-wave trough (Takaya and Nakamura 2005b). Relative importance of each of the energy conversion/generation terms is likely to vary in the course of the life cycle of a sub-monthly event of the WP pattern, which will be studied in our future study.

Previous studies have pointed out a linkage between the WP pattern and ENSO (e.g., Horel and Wallace 1981; Kodera 1998), which suggests that the WP pattern can be forced remotely by ENSO. As shown in Appendix C, however, the ENSO-WP relationship is not necessarily strong, suggesting that the WP pattern can emerge solely through internal atmospheric dynamics as a dynamical mode even without remote influence of ENSO. We also need to clarify the impacts of global warming on the WP pattern, in recognition of its influence on both the East Asian winter monsoon and the ozone variability in the polar stratosphere. The findings of the present study may lead us to the speculation that the WP pattern may undergo some modulations by the projected weakening of thermal contrasts between the Asian Continent and the Pacific. Detailed analysis on any possible projected changes in the structure and/or dynamics of the WP pattern will be presented in another paper.

Acknowledgments

This study is supported in part by the Japanese Ministry of Environment through the Environment Research and Technology Development Funds A-1201 and 2-1503, by Japanese Ministry of Education, Culture, Sports, Science and Technology (MEXT) through the Arctic GRENE and ArCS projects and through a Grant-in-Aid for Scientific

Research in Innovative Areas 2205, and by the Japan Society for the Promotion of Science (JSPS) through a Grant-in-Aid for Scientific Research (B) 25287120. K.N. is also supported by JSPS through a Grant-in-Aid for Young Scientists (B) 25800261. The JRA-25 dataset is provided by the Japan Meteorological Agency and the Central Research Institute of Electric Power Industry. The Grid Analysis and Display System (GrADS) was used for drawing figures. The NCEP Reanalysis data is provided by the NOAA/OAR/ESRL PSD from their web site at http://www.esrl.noaa.gov/psd/

Appendix A: Partial correlation

Consider three variables of X_i, Y_i, and Z_i, and linear regression equations among them:

$$X_i = a_x\, Z_i + b_x + \epsilon_{xi},$$

$$Y_i = a_y Z_i + b_y + \epsilon_{yi}\ ,$$

where a_x, b_x, a_y, and b_y are constant. Then residuals ε_{xi} and ε_{yi} are not correlated with Z_i. Correlation between ε_{xi} and ε_{yi} is the partial correlation between X_i and Y_i without any influence of Z_i. In the calculation of teleconnectivity where variability of the PNA pattern is removed, X and Y correspond to geopotential height at a given pair of grid points, while Z correspond to the PNA index, and the teleconnectivity is based on the correlation between ε_{xi} and ε_{yi} instead of that between X and Y.

Appendix B: Derivation of $\boldsymbol{CK_{HF}}$ in (6)

In the following, derivation of CK_{HF} in (6) is described. CP_{HF} in (7) may be derived in a similar manner. We start with the following quasi-geostrophic momentum equations in pressure coordinate:

$$\frac{\partial u}{\partial t} + u\frac{\partial u}{\partial x} + v\frac{\partial u}{\partial y} - fv = -\frac{\partial \phi}{\partial x}, (B1)$$

$$\frac{\partial v}{\partial t} + u\frac{\partial v}{\partial x} + v\frac{\partial v}{\partial y} + fu = -\frac{\partial \phi}{\partial y}. (B2)$$

Here ϕ designates geopotential. We now have all the variables separated into monthly mean (overbars with superscript m) and higher frequency component (double primes), which yields

$$\frac{\partial \bar{u}^m}{\partial t} + \frac{\partial u''}{\partial t} + \bar{u}^m\frac{\partial \bar{u}^m}{\partial x} + u''\frac{\partial \bar{u}^m}{\partial x} + \bar{u}^m\frac{\partial u''}{\partial x} + u''\frac{\partial u''}{\partial x} + \bar{v}^m\frac{\partial \bar{u}^m}{\partial y} + v''\frac{\partial \bar{u}^m}{\partial y} + \bar{v}^m\frac{\partial u''}{\partial y}$$
$$+ v''\frac{\partial u''}{\partial y} - f\bar{v}^m - fv'' = -\frac{\partial \bar{\phi}^m}{\partial x} - \frac{\partial \phi''}{\partial x}. \quad (B3)$$

Furthermore, applying division of monthly-mean quantities into their climatological means (overbars) and deviations from them (i.e., anomalies; denoted with primes) to (B3) yields,

$$\frac{\partial \bar{u}}{\partial t} + \frac{\partial u'}{\partial t} + \bar{u}\frac{\partial \bar{u}}{\partial x} + u'\frac{\partial \bar{u}}{\partial x} + \bar{u}\frac{\partial u'}{\partial x} + u'\frac{\partial u'}{\partial x} + \overline{u''\frac{\partial u''}{\partial x}} + \left(u''\frac{\partial u''}{\partial x}\right)' + \bar{v}\frac{\partial \bar{u}}{\partial y} + v'\frac{\partial \bar{u}}{\partial y}$$
$$+ \bar{v}\frac{\partial u'}{\partial y} + v'\frac{\partial u'}{\partial y} + \overline{v''\frac{\partial u''}{\partial y}} + \left(v''\frac{\partial u''}{\partial y}\right)' - f\bar{v} - fv'$$
$$= -\frac{\partial \bar{\phi}}{\partial x} - \frac{\partial \phi'}{\partial x}. \quad (B4)$$

Taking the climatological averaging of (B4) yields:

$$\frac{\partial \bar{u}}{\partial t} + \bar{u}\frac{\partial \bar{u}}{\partial x} + \overline{u'\frac{\partial u'}{\partial x}} + \overline{u''\frac{\partial u''}{\partial x}} + \bar{v}\frac{\partial \bar{u}}{\partial y} + \overline{v'\frac{\partial u'}{\partial y}} + \overline{v''\frac{\partial u''}{\partial y}} - f\bar{v} = -\frac{\partial \bar{\phi}}{\partial x}. \quad (B5)$$

Subtracting (B5) from (B4) leads to:

$$\frac{\partial u'}{\partial t}+u'\frac{\partial \bar{u}}{\partial x}+\bar{u}\frac{\partial u'}{\partial x}+u'\frac{\partial u'}{\partial x}-\overline{u'\frac{\partial u'}{\partial x}}+\left(u"\frac{\partial u"}{\partial x}\right)'+v'\frac{\partial \bar{u}}{\partial y}+\bar{v}\frac{\partial u'}{\partial y}+v'\frac{\partial u'}{\partial y}-\overline{v'\frac{\partial u'}{\partial y}}$$
$$+\left(v"\frac{\partial u"}{\partial y}\right)'-fv'=-\frac{\partial \phi'}{\partial x}. (B6)$$

Multiplying (B6) with *u*’ and neglecting cubic terms of monthly anomalies (primes) yield:

$$\frac{\partial}{\partial t}\left(\frac{u'^2}{2}\right)=-u'u'\frac{\partial \bar{u}}{\partial x}-u'v'\frac{\partial \bar{u}}{\partial y}-u'\left(\frac{\partial u"u"}{\partial x}+\frac{\partial u"v"}{\partial y}\right)'-\bar{u}\frac{\partial}{\partial x}\left(\frac{u'^2}{2}\right)-\bar{v}\frac{\partial}{\partial y}\left(\frac{u'^2}{2}\right)$$
$$+fu'v'-u'\frac{\partial \phi'}{\partial x}. \quad (B7)$$

Similar manipulations applied to (B2) lead to:

$$\frac{\partial}{\partial t}\left(\frac{v'^2}{2}\right)=-u'v'\frac{\partial \bar{v}}{\partial x}-v'v'\frac{\partial \bar{v}}{\partial y}-v'\left(\frac{\partial v"v"}{\partial y}+\frac{\partial u"v"}{\partial x}\right)'-\bar{u}\frac{\partial}{\partial x}\left(\frac{v'^2}{2}\right)-\bar{v}\frac{\partial}{\partial y}\left(\frac{v'^2}{2}\right)$$
$$-fu'v'-v'\frac{\partial \phi'}{\partial y}. \quad (B8)$$

We assume that the climatological-mean wind is non-divergent, then

$$\frac{\partial \bar{u}}{\partial x}=-\frac{\partial \bar{v}}{\partial y}.$$

Advection of geopotential by monthly anomalies can be written as follows:

$$-u'\frac{\partial \phi'}{\partial x}-v'\frac{\partial \phi'}{\partial y}=-u_g{}'\frac{\partial \phi'}{\partial x}-u_a{}'\frac{\partial \phi'}{\partial x}-v_g{}'\frac{\partial \phi'}{\partial y}-v_a{}'\frac{\partial \phi'}{\partial y}$$
$$=-\frac{\partial u_a{}'\phi'}{\partial x}-\frac{\partial v_a{}'\phi'}{\partial y}+\phi'\left(\frac{\partial u_a{}'}{\partial x}+\frac{\partial v_a{}'}{\partial y}\right)$$
$$=-\frac{\partial u_a{}'\phi'}{\partial x}-\frac{\partial v_a{}'\phi'}{\partial y}-\phi'\frac{\partial \omega'}{\partial p}$$
$$=-\frac{\partial u_a{}'\phi'}{\partial x}-\frac{\partial v_a{}'\phi'}{\partial y}-\frac{\partial \omega'\phi'}{\partial p}+\omega'\frac{\partial \phi'}{\partial p}=-\nabla\cdot(\boldsymbol{V}_a{}'\phi')-\omega'\frac{RT'}{p}$$

Here, $\boldsymbol{V}_a{}'$ denotes anomalous three-dimensional ageostrophic motion, and the subscripts g and a signify the geostrophic and ageostrophic wind components, respectively. By combining (B7) and (B8) and utilizing the above expression, we have finally obtained the following equation that describes local time tendency of kinematic energy of monthly anomalies (*KE*):

$$\frac{\partial(KE)}{\partial t} = CK + CK_{HF} - \omega'\frac{RT'}{p} - \nabla\cdot(\boldsymbol{V}_a{}'\phi') - \frac{\partial}{\partial x}\left(\bar{u}(KE)\right) - \frac{\partial}{\partial y}\left(\bar{v}(KE)\right). \quad (B9)$$

The first two terms CK and CH_{HF} on RHS are defined in (3) and (6), respectively. The third term represents the conversion from *APE* to *KE*, which needs not be considered in discussing the total energy (*APE* + *KE*), as in our analysis. The fourth term denotes the convergence of ageostrophic geopotential flux associated with propagation of stationary Rossby waves in monthly-mean anomaly fields, and the last two terms together represent the horizontal convergence of the (advective) *KE* flux associated with the climatological-mean flow. These flux terms represent spatial redistribution of *KE* by circulation and thus make no net contribution to the energetics if integrated three-dimensionally over the hemisphere as in Table 2.

Appendix C: The WP pattern and ENSO

Here, we verify a linkage between the WP pattern and ENSO, which have been pointed out by previous studies (e.g., Horel and Wallace 1981; Kodera 1998), but for a longer period. To do so, we classified the 186 winter months (DJF) in the period of 1949/50 – 2010/11, according to phases of the WP pattern (i.e., positive, negative, and neutral) and ENSO (El Niño, La Niña, and neutral). In any of the months of the positive (negative) phase of the WP pattern chosen for the following analysis, the WP index defined in (1) exceeds a unit standard deviation positively (negatively). The other classification of the winter months is based on two definitions of ENSO events used operationally by the Japan Meteorology Agency (JMA) and National Oceanic and Atmospheric Administration / Climate Prediction Center (NOAA/CPC) (Table A1). According to the JMA definition, the occurrence of an El Niño (a La Niña) event is officially identified when 5-month moving averaged Niño 3 index, defined as the SST anomaly averaged within [5 ˚S~5 ˚N, 150 ˚W~90 ˚W], is 0.5 ˚C (–0.5 ˚C) or higher (lower) for at least 6 consecutive months. Likewise, the definition by NOAA/CPC of an El Niño (a La Niña) event is such that 3-month moving averaged Niño 3.4 index, defined as the SST anomaly averaged within [5 ˚S - 5 ˚N, 170 ˚W - 120 ˚W], exceeds 0.5 (is below -0.5). As shown in Table A1, those two definitions yield only slight differences, and therefore the discussion below is based mainly on the JMA definition.

Table A1 indicates that only a single monthly event of the positive WP pattern was observed during El Niño, which is much fewer than during La Niña (13 months). The negative WP events were more frequent during El Niño (10 months) than during La Niña (6 months). In other words, El Niño tends to set conditions highly unfavorable for the occurrence of the positive phase of the WP pattern, while La Niña tends to set conditions unfavorable for the occurrence of the negative WP pattern. These results seem consistent with previous studies (Horel and Wallace 1981; Trenberth et al. 1998), but Table A1 indicates that the positive WP pattern was observed most frequently when the Tropical Pacific SST is close to normal (i.e., neutral). In other words, the linkage between the WP pattern and ENSO is not particularly strong, and the WP pattern can develop through internal atmospheric dynamics as a dynamical mode even without remote influence of ENSO. Table A1 nevertheless shows that ENSO is still influential in determining which phase of the WP pattern is likely to be triggered. In addition, recent studies have suggested that SST anomalies in the western North Pacific (Frankignoul et al. 2011; Hurwitz et al. 2012) and/or in the Sea of Japan (Hirose et al. 2009) may trigger the WP pattern. Further study is necessary on the mechanisms behind the linkage between the WP pattern and SST variability both in the Tropics and extratropics.

References

Adler, R. F., and Coauthors, 2003: The version-2 Global Precipitation Climatology Project (GPCP) monthly precipitation analysis (1979–present). *J. Hydrometeor.,* **4**, 1147–1167.

Black, R. X., and R. M. Dole, 1993: The dynamics of large-scale cyclogenesis over the North Pacific Ocean. *J. Atmos. Sci.*, **50**, 421-442.

Black, R. X., 1997: Deducing anomalous wave source regions during the life cycles of persistent flow anomalies. *J. Atmos. Sci.* **54**. 895-907.

Blackmon, M. L., R. A. Madden, J. M. Wallace, and D. S. Gutzler, 1979: Geographical variations in the vertical structure of geopotential height fluctuations. *J. Atmos. Sci.*, **36**, 2450–2466.

Blackmon, M. L., Y. -H. Lee, and J. M. Wallace, 1984: Horizontal structure of 500 mb height fluctuations with long, intermediate and short time scales. *J. Atmos. Sci.* **41**.

961-979.

Dee, D. P., and Coauthors, 2011: The ERA-Interim reanalysis: configuration and performance of the data assimilation system. *Quart. J. Roy. Meteor. Soc.,* **137**, 553-597.

Frankignoul, C., and N. Sennéchael, Y.-O. Kwon, M. A. Alexander, 2011: Influence of the meridional shifts of the Kuroshio and the Oyashio Extensions on the atmospheric circulation. *J. Climate*, **24**, 762-777.

Feldstein, S. B., 2003: The dynamics of NAO teleconnection pattern growth and decay. *Quart. J. Roy. Meteor. Soc.,* **129**, 901-924.

Hirose, N., K. Nishimura, and M. Yamamoto, 2009: Observational evidence of a warm ocean current preceding a winter teleconnection pattern in the northwestern Pacific. *Geophys. Res. Lett.*, **36**, L09705, doi:10.1029/2009GL037448.

Horel, J. D., and J. M. Wallace, 1981: Planetary-scale atmospheric phenomena associated with the Southern Oscillation. *Mon. Wea. Rev.*, **109**, 813–829.

Hoskins, B. J., I. James, and G. H. White, 1983: The shape, propagation and mean-flow interaction of large-scale weather systems. *J. Atmos. Sci.*, **40**, 1595-1612.

Hurwitz, M. M., P. A. Newman, and C. I. Garfinkel, 2012: On the influence of North Pacific sea surface temperature on the Arctic winter climate. *J. Geophys. Res.*, **117**, D19110, doi:10.1029/2012JD017819.

Hsu, H. -H., and J. M. Wallace, 1985: Vertical structure of wintertime teleconnection patterns in Northern Hemisphere. *J. Atmos. Sci.*, **42**, 1693-1710.

Ishii, Y., and K. Hanawa, 2005: Large-scale variabilities of wintertime wind stress curl field in the North Pacific and their relation to atmospheric teleconnection patterns. *Geophys. Res. Lett.*, **32**, L10607, doi:10.1029/2004GL022330.

Kalnay, E., and Coauthors, 1996: The NCEP/NCAR 40-year reanalysis project. *Bull. Amer. Meteor. Soc.*, **77**, 437-471.

Kodera, K. Consideration of the origin of the different midlatitude atmospheric responses among El Nino events. *J. Meteor. Soc. Japan*, **76**, 347-361.

Koide, H., and K. Kodera, 1999: A SVD analysis between the winter NH 500-hPa height and surface temperature fields. *J. Meteor. Soc. Japan*, **77**, 47-61.

Kosaka, Y., and H. Nakamura, 2006: Structure and dynamics of the summertime Pacific-Japan (PJ) teleconnection pattern. *Quart. J. Roy. Meteor. Soc.,* **132,** 2009-2030.

Kosaka, Y., and H. Nakamura, 2010: Mechanisms of meridional teleconnection observed between a summer monsoon system and a subtropical anticyclone. Part I: The Pacific-Japan pattern. *J. Climate*, **23**, 5085-5108.

Kushnir, K., and J. M. Wallace, 1989: Low-frequency variability in the Northern Hemisphere winter: geographical distribution, structure and time-scale dependence. *J. Atmos. Sci*., **46**, 3122–3143.

Lau, N.-C., 1988: Variability of the observed midlatitude storm tracks in relation to low-frequency changes in the circulation pattern. *J. Atmos. Sci*., **45**, 2718-2743.

Lau, N.-C., and M. J. Nath, 1991: Variability of the baroclinic and barotropic transient eddy forcing associated with monthly changes in the midlatitude storm tracks. *J. Atmos. Sci*., **48**, 2589-1613.

Lee, S., and H.-K. Kim, 2003: The dynamical relationship between subtropical and eddy-driven jets. *J. Atmos. Sci*., **60**, 1490– 1503.

Linkin, M. E., and S. Nigam, 2008: The North Pacific Oscillation-West Pacific teleconnection pattern: Mature-phase structure and winter impacts. *J. Climate,* **21**, 1979–1997.

Li, C., and J. J. Wettstein, 2012: Thermally driven and eddy driven jet variability in reanalysis. *J. Climate,* **25**, 1587-1596.

Michel, C., and G. Rivière, 2011: The link between Rossby wave breakings and weather regime transitions. *J. Atmos. Sci.*, **68**, 1730-1748.

Mohri, K., 1953: On the fields of wind and temperature over Japan and adjacent waters during winter of 1950-1951. *Tellus,* **3**, 340-358.

Nakamura, H., and T. Sampe, 2002: Trapping of synoptic-scale disturbances into the North-Pacific subtropical jet core. *Geophys. Res. Lett.,* **29**, doi: 1029/2002GL015335.

Nakamura, H., M. Tanaka, and J. M. Wallace 1987: Horizontal structure and energetics of Northern Hemisphere wintertime teleconnection patterns. *J. Atmos. Sci.*, **44**, 3377-3391.

Nakamura, H., T. Izumi, and T. Sampe, 2002: Interannual and decadal modulations recently observed in the Pacific storm track activity and East Asian winter monsoon. *J. Climate*, **15**, 1855–1874.

Nakamura, H., T. Miyasaka, Y. Kosaka, K. Takaya, and M. Honda, 2010: Northern Hemisphere extratropical tropospheric planetary waves and their low-frequency variability: Their vertical structure and interaction with transient eddies and surface thermal contrasts, in Chap. 6 of *Climate Dynamics: Why Does Climate Vary?*, D. Sun and F. Bryan, Eds., *AGU Geophys. Monogr.*, **189**, 149-179.

Nishii, K., H. Nakamura, and Y. J. Orsolini, 2010: Cooling of the wintertime Arctic stratosphere induced by the Western Pacific teleconnection pattern. *Geophys. Res. Lett*., **37**, L13805, doi:10.1029/2010GL043551.

Nitta, T., 1987: Convective activities in the tropical western Pacific and their impact on the Northern Hemisphere summer circulation. *J. Meteor. Soc. Japan,* **65**, 373-390.

Onogi, K., and Coauthors, 2007: The JRA-25 reanalysis. *J. Meteor. Soc. Japan,* **85**, 369-432.

Orsolini, Y. J., A. Y. Karpechko, and G. Nikulin, 2009: Variability of the Northern Hemisphere polar stratospheric cloud potential: The role of North Pacific disturbances. *Quart. J. Roy. Meteor. Soc.*, **135**, 1020-1029.

Ose, T., 2000: A biennially oscillating sea surface temperature and the Western Pacific Pattern. *J. Meteor. Soc. Japan*, **78**, 98-99.

Pavan, V., Tibaldi, S., and Branković, Č., 2000: Seasonal prediction of blocking frequency: Results from winter ensemble experiments. *Quart. J. Roy. Meteor. Soc.*, **126**, 2125–2142.

Pedlosky, J., 1987: Geophysical Fluid Dynamics. 2nd ed. Springer, 710 pp.

Rayner, N. A., D. E. Parker, E. B. Horton, C. K. Folland, L. V. Alexander, D. P. Rowell, E. C. Kent, and A. Kaplan, 2003: Global analyses of sea surface temperature, sea ice, and night marine air temperature since the late nineteenth century. *J. Geophys. Res.*, **108**, 4407, doi:10.1029/2002JD002670.

Rivière, G., 2010: Role of Rossby wave breaking in the West Pacific teleconnection. *Geophys. Res. Lett.*, **37**, L11802, doi:10.1029/2010GL043309.

Robinson, W. A., 1991: The dynamics of low-frequency variability in a simple model of the global atmosphere. *J. Atmos. Sci.*, **48**, 429-441.

Rogers, J. C., 1981: The North Pacific Oscillation. *J. Climatol*., **1**, 39–57.

Sugimoto, H., and K. Hanawa, 2009: Decadal and interdecadal variations of the Aleutian low activity and their relation to upper oceanic variations over the North Pacific. *J. Meteor. Soc. Japan,* **87***,* 601-614.

Sheng, J., and J. Derome, 1991: An observational study of the energy transfer between the seasonal mean flow and transient eddies. *Tellus A*, **43**, 128–144.

Simmons, A. J., J. M. Wallace, and G. W. Branstator, 1983: Barotropic wave propagation and instability, and atmospheric teleconnection patterns. *J. Atmos. Sci.*, **40**, 1363-1392.

Takaya, K., and H. Nakamura, 2005a: Mechanisms of intraseasonal amplification of the cold Siberian High. *J. Atmos. Sci.*, **62**, 4423-4440.

Takaya, K., and H. Nakamura, 2005b: Geographical dependence of upper-level blocking formation associated with intraseasonal amplification of the Siberian High. *J. Atmos. Sci.,* **62**, 4441-4449.

Takaya, K., and H. Nakamura, 2013: Interannual variability of the East Asian winter monsoon and associated modulations of the planetary waves. *J. Climate*, **26**, 9445-9461.

Trenberth, K. E., G. W. Branstator, D. Karoly, A. Kumar, N.-C. Lau, and C.

Ropelewski, 1998: Progress during TOGA in understanding and modeling global teleconnections associated with tropical sea surface temperatures. *J. Geophys. Res.*, **103**, 14,291–14,324.

Walker, G. T., and E. W. Bliss, 1932: World weather V. *Mem. Roy. Meteor. Soc*., **4**, 53–84.

Wallace, J. M., and D. S. Gutzler, 1981: Teleconnections in the geopotential height field during the Northern Hemisphere winter. *Mon. Wea. Rev*. **109**, 784-812.

Yamamoto, M., and Hirose, 2009: Possible modification of atmospheric circulation over the northwestern Pacific induced by a small semi-enclosed ocean. *Geophys. Res. Lett.*, **38**, L03804, doi:10.1029/2010GL046214.

Table 1. The 18 and 14 months selected for composites of the positive and negative phases, respectively, of the WP pattern.

Positive	Negative
Jan. 1980	Dec. 1982
Dec. 1980	Jan. 1987
Feb. 1982	Dec. 1987
Jan. 1984	Jan. 1988
Feb. 1984	Jan. 1989
Feb. 1985	Feb. 1989
Feb. 1986	Jan. 1990
Dec. 1989	Feb. 1990
Jan. 1991	Jan. 1992
Feb. 1991	Feb. 1999
Feb. 1994	Feb. 2001
Feb. 1995	Feb. 2006
Dec. 1995	Dec. 2006
Jan. 1997	Jan. 2007
Feb. 2003	
Jan. 2004	
Dec. 2005	
Dec. 2010	

Table 2. Efficiency (day^{-1}) of each of the conversion/generation terms CK, CP, CQ, CK_{HF}, and CP_{HF}, represented in (3) through (7), respectively, in the text. The efficiency represents how fast a particular term alone could replenish the total energy (KE + APE) based on composited monthly-mean anomalies associated with the WP pattern. The total energy and the respective conversion/generation terms are integrated horizontally over the entire extratropical North Hemisphere (20˚ ~ 90˚N, 0˚ ~ 360˚E) and vertically from the surface to the 100-hPa level. "*CPK*" represents the efficiency (day^{-1}) of conversion from APE to KE (the third term of RHS of (B9)) divided by the total energy. "Positive (negative) WP" signifies the efficiency evaluated for the positive (negative) WP pattern.

	Positive WP	Negative WP
CK	0.062	0.048
CP	0.220	0.243
CQ	-0.106	-0.113
CK_{HF}	0.090	0.093
CP_{HF}	-0.065	-0.065
CPK	-0.005	0.023

Table A1. Classification of the 186 winter months (DJF) in the period 1949/50 - 2010/11 according to phases of the WP pattern and ENSO. Calculation of the WP pattern index is based on (1), which was applied to the NCEP-R1 data. The numbers in parentheses are statistics based on the ENSO definition by NOAA/CPC, while others are based on the definition by JMA.

	El Niño	Neutral	La Niña
WP positive	1(2)	18(19)	13(11)
WP neutral	31(44)	67(42)	32(44)
WP negative	10(14)	8(6)	6(5)

Figure captions

Figure 1. Map of teleconnectivity (contoured for every 0.05 for no less than 0.5) evaluated from monthly 500-hPa height anomalies based on the NCEP-R1 data for winters (DJF) of (a) 1962/63 – 1976/77, the same period as in WG81, and (b) 1948/49 – 2010/11. (c) Same as in (b), but the teleconnectivity is based on partial correlation from which the variability associated with the PNA pattern is excluded. Coloring is to highlight the maxima (contoured for 0.65 and 0.8). Note that significance levels of the teleconnectivity (i.e., negative correlation) at 0.01 evaluated by the Student's *t*-test on the correlation coefficients with (a) 43 and (b, c) 187 degrees of freedom assumed, are 0.39 and 0.18, respectively. The centers of action of the WP pattern are indicated by a pair of red crosses at (30˚N, 155˚E) and (60˚N, 155˚E). The two blue crosses in (c) denote another pair of teleconnectivity maxima that are mutually correlated.

Figure 2. Monthly height anomalies (contoured for every 20 m; dashed for negative) composited for the 18 and 14 strongest months of (a, c, e) positive and (b, d, f) negative phases, respectively, of the WP pattern. Yellow (blue) shading represents the anomalies that are positively (negatively) significant at the 95% confidence level based on the *t*-statistic. Green dots represent the reference grid points at (30˚N, 155˚E) and (60˚N, 155˚E) used for the definition of the WP index. (a, b) 500-hPa height anomalies over the Asian-Pacific region (20˚N~90˚N, 65˚E~115˚W). (c, d) Zonal-height sections for 30˚N (the latitude close to the southern reference grid point for the WP index (WG81)). (e, f) Meridional sections for 155˚E (the longitude for the two reference grid points for the WP index). Zero lines are omitted. Red and blue crosses in (c-f) signify ridges and troughs, respectively. The longitude of 180˚ and the latitude of 60˚N are highlighted

with bold vertical lines in (c, d) and (e, f), respectively.

Figure 3. As in Fig. 2a, but for (a) temperature anomalies at the lowest model level (σ = 0.995) (countered for every 0.5 K), (b c) temperature anomalies (countered for every 0.5 K) at the 850-hPa (b) and (c) 500-hPa levels, (d) 250-hPa zonal wind anomalies (2 m s^{-1}), (e) 850-hPa anomalous heat flux due to transient eddies (2 K m s^{-1}), and (f) variance of 250-hPa meridional wind fluctuations associated with transient eddies (10 m^2 s^{-2}). Zero lines are omitted. In (a), vectors represent the total (anomaly + climatology) wind associated with the WP pattern at the lowest model level. In (b, c), vectors represent the wind anomalies associated with the monthly WP pattern at the corresponding levels. Brown line in (d-f) indicates (d) climatological jet axis, (e) 12 m s^{-1}, and (f) 150 m^2 s^{-2} of corresponding climatological-mean fields.

Figure 4. As in Fig. 2a, but for (a) anomalous diabatic heating at the 850-hPa level (contoured for every 0.5 K day^{-1}), (b) SST anomalies (0.2 K), (c) anomalous upward surface sensible heat flux (5 W m^{-2}), (d) anomalous diabatic heating at the 500-hPa level (0.5 K day^{-1}), and (e) precipitation anomalies of GPCP (0.3 mm day^{-1}). Zero lines are omitted.

Figure 5. (a) Local barotropic KE conversion (CK) at the 250-hPa level (shading; 10^{-4} m^2 s^{-3}) associated with the positive WP pattern. Brown contours represent

climatological-mean zonal wind (contoured for 30, 40, 50 m s^{-1}, …) in winter (DJF). (b) As in (a), but for the KE conversion related only to the diffluence/confluence of the climatological-mean jet (*CKx*). Arrows are for 250-hPa wind anomalies (m s^{-1}) associated with the WP pattern. (c) As in (b), but for the KE conversion related mainly to the meridional shear of the climatological-mean jet (*CKy*).

Figure 6. (a, b) Local baroclinic APE conversion (*CP*) at the (a) 500-hPa and (b) 850-hPa levels (shading; 10^{-4} m^2 s^{-3}) associated with the positive WP pattern. Contours represent the climatological-mean temperature (every 10 K) at the given level. (c, d) As in (a, b), respectively, but for APE conversion related only to the zonal gradient of the climatological-mean temperature (*CPx*). (e, f) As in (a, b), respectively, but for APE conversion related only to the meridional gradient of the climatological-mean temperature (*CPy*).

Figure 7. APE generation (shading; 10^{-4} m^2 s^{-3}) by anomalous diabatic heating (*CQ*) at the (a) 500-hPa and (b) 850-hPa levels, associated with the positive WP pattern.

Figure 8. (a) Local barotropic KE generation as feedback forcing by anomalous activity of transient eddies (CK_{HF}) at the 250-hPa level (shading; 10^{-4} m^2 s^{-3}) associated with the positive WP pattern. (b) As in (a), but for baroclinic APE generation as feedback forcing by anomalous activity of transient eddies (CP_{HF}) at the 850-hPa level. (c) Anomalous flux of westerly momentum at the 250-hPa level associated with transient

eddies (arrows) and its convergence (shading; m s^{-2}). Contours represent monthly-mean 250-hPa zonal wind anomalies (every 4 m s^{-1}; dashed for anomalous easterlies; zero lines are thickened) associated with the positive WP pattern. (d) Anomalous temperature flux at the 850-hPa level associated with transient eddies (arrows) and its convergence (shading; K s^{-1} Contours represent monthly-mean 850-hPa temperature anomalies (every 1 K; dashed for negative; zero lines are thickened). (e) As in (c), but for anomalous flux of southerly momentum. Contours are for monthly-mean 250-hPa meridional wind anomalies (every 2 m s^{-1}; dashed for anomalous northerlies; zero lines are thickened).

Figure 9. Latitudinal profiles of the westerlies (m s^{-1}; left axis) and westerly momentum convergence by transient eddies (m s^{-1} $(day)^{-1}$; right axis) at the 250-hPa level along the (a-c) 155˚E and (d-f) 190˚E meridians. (a,d) Solid black line is for the climatological-mean westerlies, and dashed blue and green lines denote the corresponding profiles to which westerly anomalies composited for the positive and negative events, respectively, of the WP pattern have been added. Red solid line is the climatological-mean convergence of westerly momentum flux associated with high-frequency transient eddies. (b, e) Black line is for the westerly anomalies, and red line is for the anomalous convergence of the eddy westerly momentum flux, both composited for the positive events of the WP pattern. (c, f) As in (b, e), respectively, but for the negative events of the WP pattern.

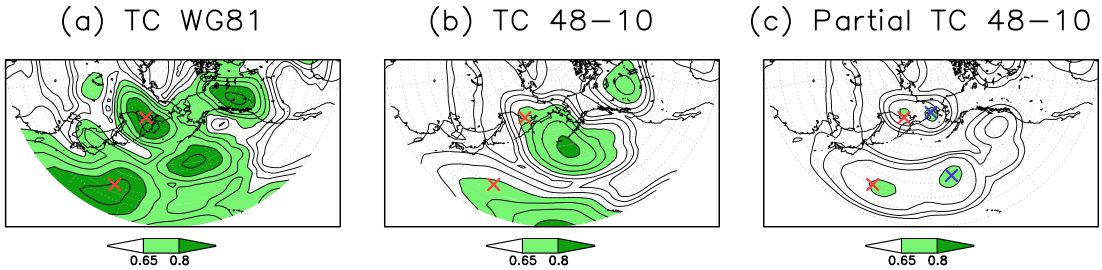

Figure 1. Map of teleconnectivity (contoured for every 0.05 for no less than 0.5) evaluated from monthly 500-hPa height anomalies based on the NCEP-R1 data for winters (DJF) of (a) 1962/63 – 1976/77, the same period as in WG81, and (b) 1948/49 – 2010/11. (c) Same as in (b), but the teleconnectivity is based on partial correlation from which the variability associated with the PNA pattern is excluded. Coloring is to highlight the maxima (contoured for 0.65 and 0.8). Note that significance levels of the teleconnectivity (i.e., negative correlation) at 0.01 evaluated by the Student's *t*-test on the correlation coefficients with (a) 43 and (b, c) 187 degrees of freedom assumed, are 0.39 and 0.18, respectively. The centers of action of the WP pattern are indicated by a pair of red crosses at (30°N, 155°E) and (60°N, 155°E). The two blue crosses in (c) denote another pair of teleconnectivity maxima that are mutually correlated.

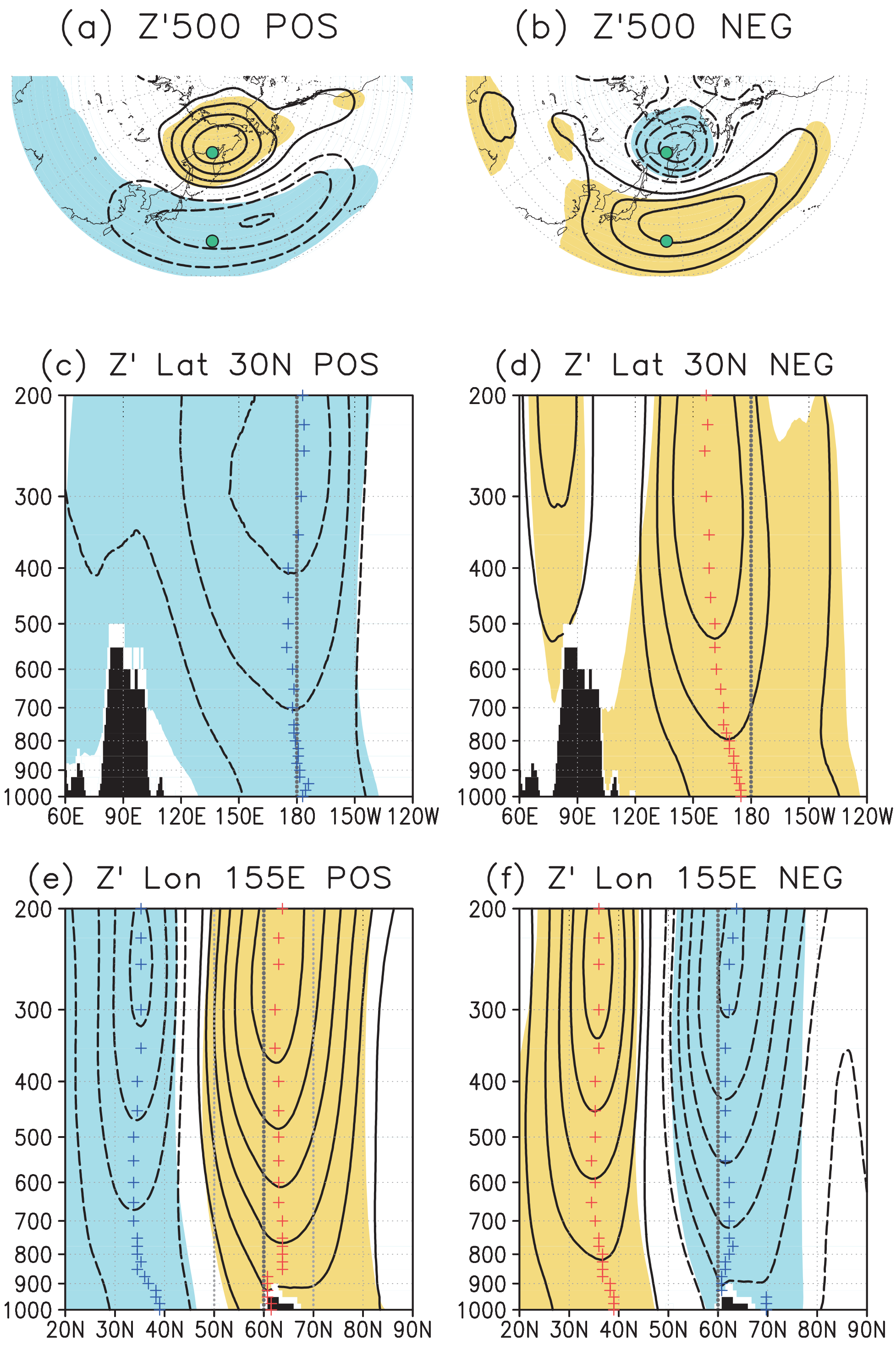

Figure 2. Monthly height anomalies (contoured for every 20 m; dashed for negative) composited for the 18 and 14 strongest months of (a, c, e) positive and (b, d, f) negative phases, respectively, of the WP pattern. Yellow (blue) shading represents the anomalies that are positively (negatively) significant at the 95% confidence level based on the

t-statistic. Green dots represent the reference grid points at (30˚N, 155˚E) and (60˚N, 155˚E) used for the definition of the WP index. (a, b) 500-hPa height anomalies over the Asian-Pacific region (20˚N~90˚N, 65˚E~115˚W). (c, d) Zonal-height sections for 30˚N (the latitude close to the southern reference grid point for the WP index (WG81)). (e, f) Meridional sections for 155˚E (the longitude for the two reference grid points for the WP index). Zero lines are omitted. Red and blue crosses in (c-f) signify ridges and troughs, respectively. The longitude of 180˚ and the latitude of 60˚N are highlighted with bold vertical lines in (c, d) and (e, f), respectively.

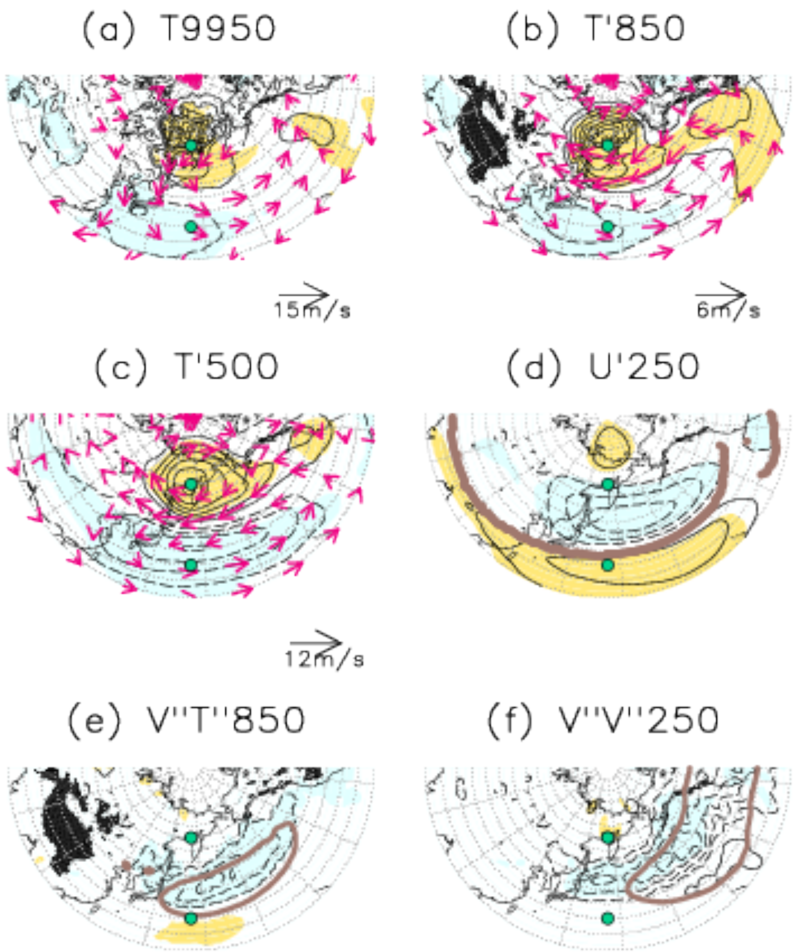

Figure 3. As in Fig. 2a, but for (a) temperature anomalies at the lowest model level (σ = 0.995) (countered for every 0.5 K), (b c) temperature anomalies (countered for every 0.5 K) at the 850-hPa (b) and (c) 500-hPa levels, (d) 250-hPa zonal wind anomalies (4 m s^{-1}), (e) 850-hPa anomalous heat flux due to transient eddies (2 K m s^{-1}), and (f) variance of 250-hPa meridional wind fluctuations associated with transient eddies (10 m^2 s^{-2}). Zero lines are omitted. In (a), vectors represent the total (anomaly + climatology) wind associated with the WP pattern at the lowest model level. In (b, c), vectors represent the wind anomalies associated with the monthly WP pattern at the corresponding levels. Brown line in (d-f) indicates (d) climatological jet axis, (e) 12 m s^{-1}, and (f) 150 m^2 s^{-2} of corresponding climatological-mean fields.

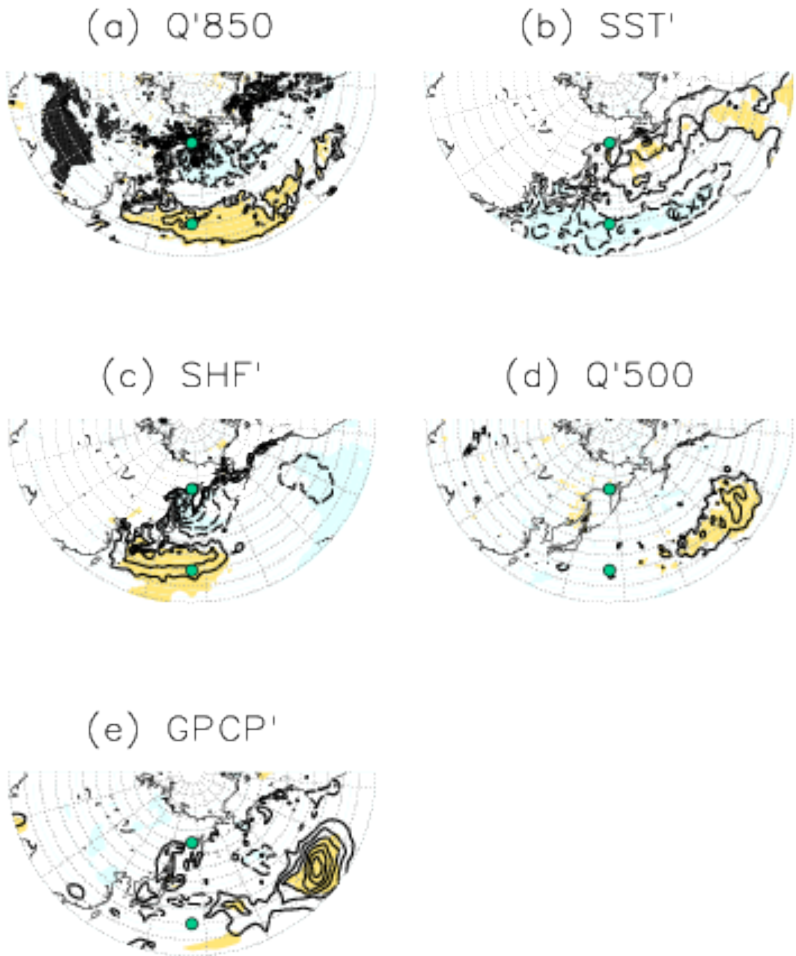

Figure 4. As in Fig. 2a, but for (a) anomalous diabatic heating at the 850-hPa level (contoured for every 0.5 K day^{-1}), (b) SST anomalies (0.2 K), (c) anomalous upward surface sensible heat flux (5 W m^{-2}), (d) anomalous diabatic heating at the 500-hPa level (0.5 K day^{-1}), and (e) precipitation anomalies of GPCP (0.3 mm day^{-1}). Zero lines are omitted.

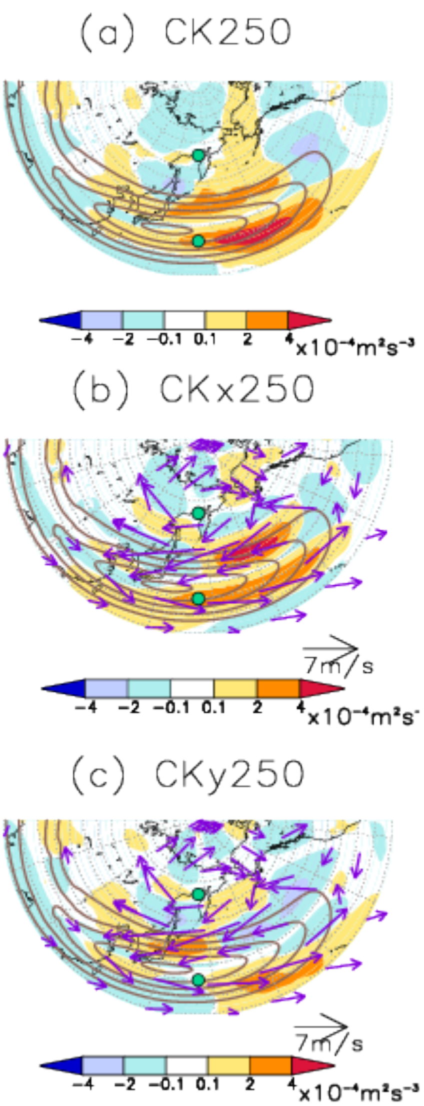

Figure 5. (a) Local barotropic KE conversion (CK) at the 250-hPa level (shading; 10^{-4} m^2 s^{-3}) associated with the positive WP pattern. Brown contours represent climatological-mean zonal wind (contoured for 30, 40, 50 m s^{-1}, …) in winter (DJF). (b) As in (a), but for the KE conversion related only to the diffluence/confluence of the climatological-mean jet (*CKx*). Arrows are for 250-hPa wind anomalies (m s^{-1}) associated with the WP pattern. (c) As in (b), but for the KE conversion related mainly to the meridional shear of the climatological-mean jet (*CKy*).

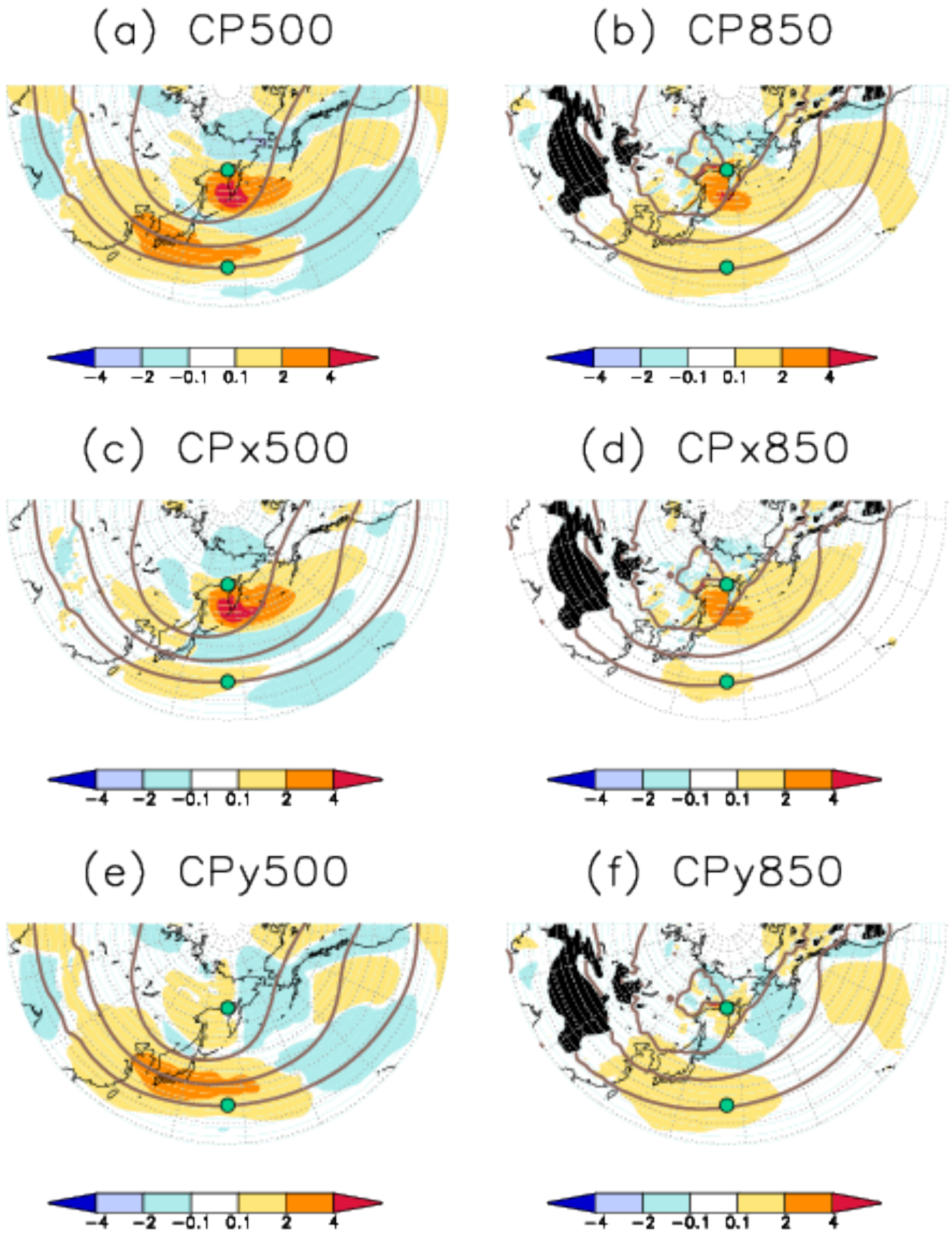

Figure 6. (a, b) Local baroclinic APE conversion (*CP*) at the (a) 500-hPa and (b) 850-hPa levels (shading; 10^{-4} m^2 s^{-3}) associated with the positive WP pattern. Contours represent the climatological-mean temperature (every 10 K) at the given level. (c, d) As in (a, b), respectively, but for APE conversion related only to the zonal gradient of the climatological-mean temperature (*CPx*). (e, f) As in (a, b), respectively, but for APE conversion related only to the meridional gradient of the climatological-mean temperature (*CPy*).

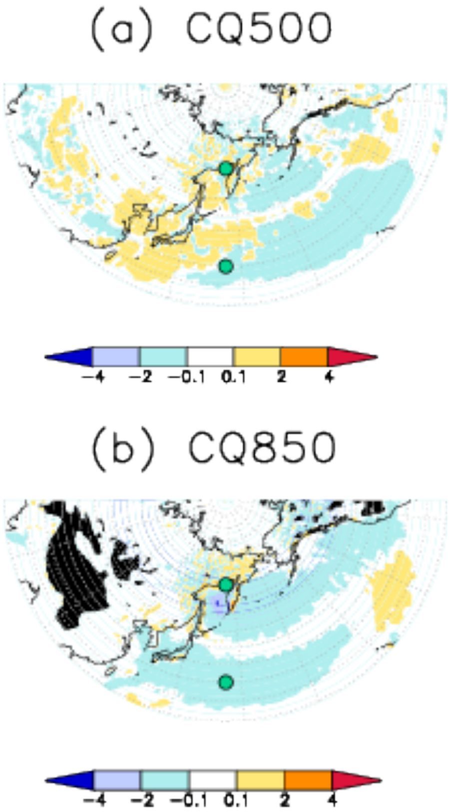

Figure 7. APE generation (shading; 10^{-4} m^2 s^{-3}) by anomalous diabatic heating (*CQ*) at the (a) 500-hPa and (b) 850-hPa levels associated with the positive WP pattern.

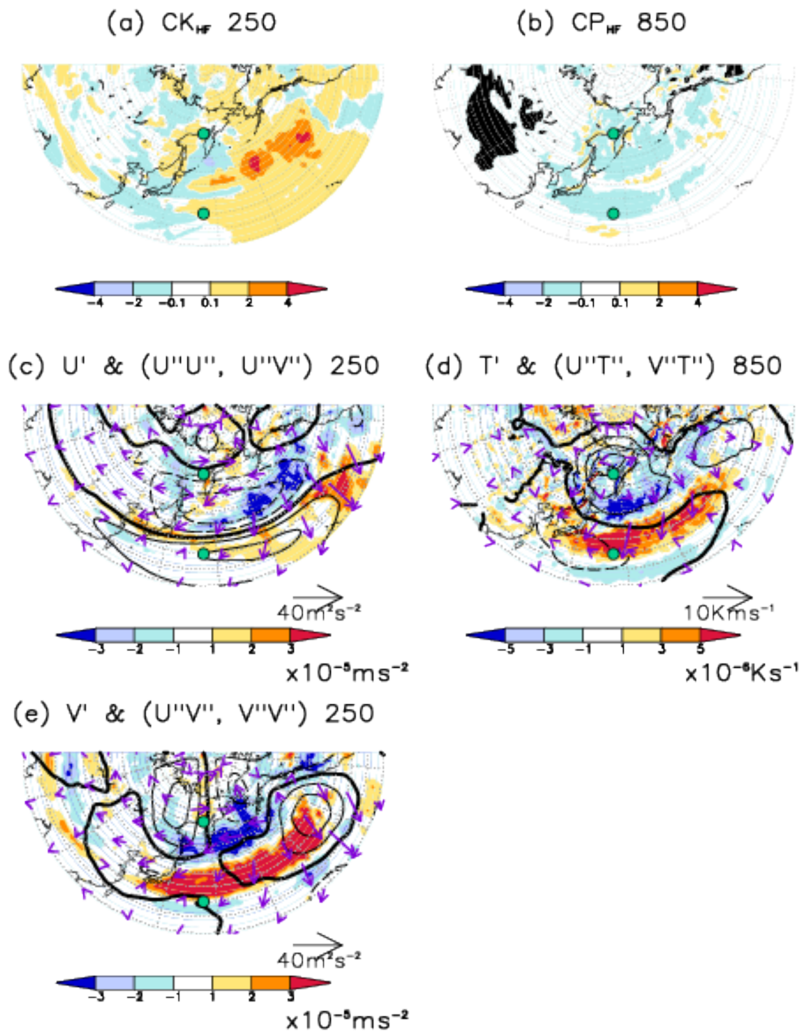

Figure 8. (a) Local barotropic KE generation as feedback forcing by anomalous activity of transient eddies (CK_{HF}) at the 250-hPa level (shading; 10^{-4} m^2 s^{-3}) associated with the positive WP pattern. (b) As in (a), but for baroclinic APE generation as feedback forcing by anomalous activity of transient eddies (CP_{HF}) at the 850-hPa level. (c) Anomalous flux of westerly momentum at the 250-hPa level associated with transient eddies (arrows) and its convergence (shading; m s^{-2}). Contours represent monthly-mean 250-hPa zonal wind anomalies (every 4 m s^{-1}; dashed for anomalous easterlies; zero lines are thickened) associated with the positive WP pattern. (d) Anomalous temperature flux at the 850-hPa level associated with transient eddies (arrows) and its convergence (shading; K s^{-1} Contours represent monthly-mean 850-hPa temperature anomalies (every 1 K; dashed for negative; zero lines are thickened). (e) As in (c), but for anomalous flux of southerly momentum. Contours are for monthly-mean 250-hPa meridional wind anomalies (every 2 m s^{-1}; dashed for anomalous northerlies; zero lines are thickened).

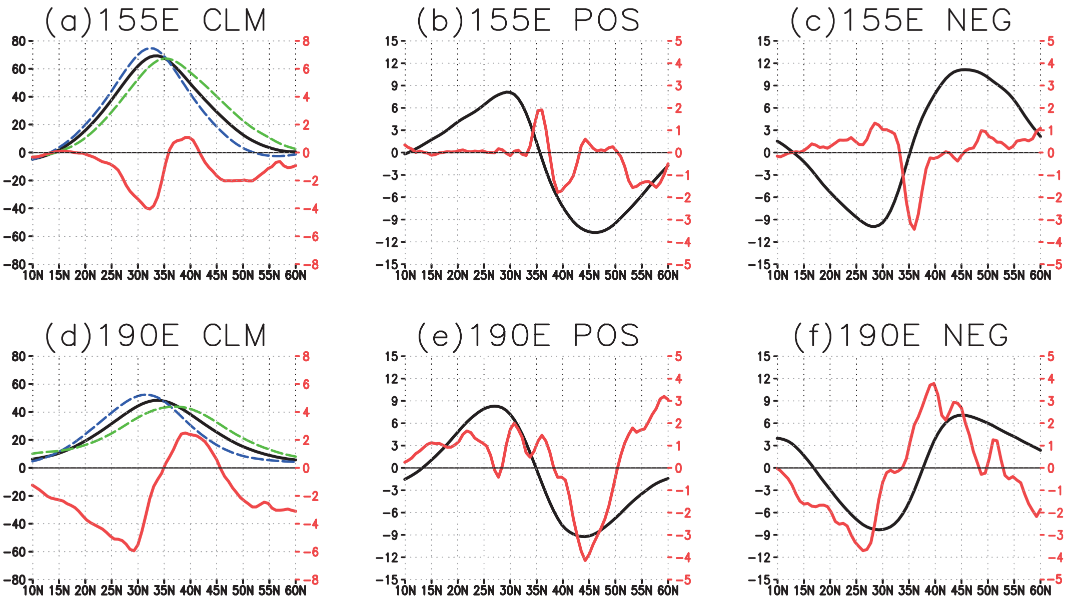

Figure 9. Latitudinal profiles of the westerlies (m s^{-1}; left axis) and westerly momentum flux convergence by transient eddies (m s^{-1} (day)$^{-1}$; right axis) at the 250-hPa level along the (a-c) 155˚E and (d-f) 190˚E meridians. (a,d) Solid black line is for the climatological-mean westerlies, and dashed blue and green lines denote the corresponding profiles to which westerly anomalies composited for the positive and negative events, respectively, of the WP pattern have been added. Red solid line is the climatological-mean convergence of westerly momentum flux associated with high-frequency transient eddies. (b, e) Black line is for the westerly anomalies, and red line is for the anomalous convergence of the eddy westerly momentum flux, both composited for the positive events of the WP pattern. (c, f) As in (b, e), respectively, but for the negative events of the WP pattern.